Postprint of: Wójcik N.A., Ali S., Möncke D., Tagiara N.S., Kamitsos E.I., Segawa H., Eriksson M., Jonson B., The influence of Be addition on the structure and thermal properties of alkali-silicate glasses, Journal of Non-Crystalline Solids, Vol. 521 (2019), 119532, DOI: 10.1016/j.jnoncrysol.2019.119532

The influence of Be addition on the structure and thermal properties of alkali-silicate glasses

N. A. Wójcik[1,2*], S. Ali[2], D. Möncke[2,3,4], N. S. Tagiara[3], E. I. Kamitsos[3], H. Segawa[2,5], M. Eriksson[6], B. Jonson[2]

[1]Department of Solid State Physics, Faculty of Applied Physics and Mathematics, Gdańsk University of Technology, Narutowicza Street 11/12, 80–233 Gdańsk, Poland

[2]Department of Built Environment and Energy Technology, Linnæus University, 35195 Växjö, Sweden

[3]Theoretical and Physical Chemistry Institute, National Hellenic Research Foundation, 48 Vassileos Constantinou Avenue, 11635 Athens, Greece

[4]Inamori School of Engineering at the New York State College of Ceramics, Alfred University, 1 Saxon Drive, Alfred, 14802, New York, USA

[5]National Institute for Materials Science, 1-1 Namiki, Tsukuba 305-0044, Japan

[6]Department of Inorganic Chemistry, Arrhenius Laboratory, Stockholm University, S-106 91 Stockholm, Sweden

**corresponding author:* natalia.wojcik@pg.edu.pl, natalia.wojcik@lnu.se

Keywords: Beryllium-containing glasses, Raman spectroscopy, IR spectroscopy, Alkali-silicate glasses, Thermal properties

Abstract

Be-Na-(Li)-Si oxide glasses containing up to 15 mol% of BeO were prepared. Their structure was characterized by X-ray powder diffraction and Raman as well as infrared spectroscopic techniques, while their chemical compositions were examined by Inductively Coupled Plasma Optical Emission Spectrometry. All materials were found to be amorphous and contain Al contaminations from minor dissolution of the alumina crucibles. The results of Raman and IR spectroscopies showed that BeO addition to Na-(Li)-Si glass systems resulted in the formation of $[BeO_{4/2}]^{2-}$ tetrahedra which are inserted into the silicate glass network, demonstrating the intermediate glass-forming role of BeO. In parallel, the effective destruction of Si-O-Si bridges was observed by vibrational spectroscopy. The glass transition temperature was studied by Differential Thermal Analysis and found to range from about 431 °C to 551 °C. A significant increase in T_g by 70 °C was found as SiO_2 was substituted by up to 15 mol% BeO.

1. Introduction

Beryllium-silicate glasses are relatively poorly studied [1-4] due to the beryllium toxicity, which requires working under a fume hood throughout preparation and melting. Another challenge are the high melting temperatures [5]. Lai and Silverman in 1928 were the first to prepare glasses of the Na_2O–BeO–SiO_2 system [1], they also reported density, refractive index, hardness and limits of ultra-violet transmission for silicate glasses containing up to 31 mol% of BeO. In 1967, glasses of the composition xBeO-(40-x)Al_2O_3-60SiO_2 (where x = 25, 30 and 34 %mol) were melted at temperatures of 1750-1800 °C by Riebling and Duke [3]. They studied density, viscosity and electrical conductance of these materials. Since that time there were only few papers; among others on the structure of binary BeO-SiO_2 glasses [6] and on the optical properties of lead-doped beryllium silicate glasses [7]. In comparison, much more attention had been given to the glass forming properties of BeF_2, which is isoelectronic to SiO_2 [8].

Glass research on beryllium-containing glasses faded in part because more favorable glass forming systems, yielding also low refractive index glasses, had been developed, and partly due to the toxicity of beryllium. However, high strength but light beryllium oxide-containing ceramics are widely used for high-speed integrated circuits, laser and electronic applications, as well as for golf clubs and bicycles. Moreover, beryllium metal is used in fusion reactors, nuclear devices, radar systems, and military infrared countermeasure devices [5]. Melting in closed systems, and using state of the art fume hoods, prevents the release of beryllium into the environment, while the element is tightly bonded in the glass. Due to the low weight and small size of the beryllium ion, BeO has been described more as a glass former than a typical glass modifier. Thus, beryllium-containing glasses are of fundamental interest in better understanding the shifting role from glass modifying to glass forming metal oxides. This paper gives new insights into the structural evolution of M_2O-SiO_2 (M=Na or Li+Na) glasses, as BeO substitutes SiO_2, and how selected glass properties change with the BeO content.

Chemically, Be^{2+} is a rather unique cation with the highest field strength (defined as charge-to-radius ratio) and the highest electronegativity among all alkaline-earth and alkali ions. Be^{2+} is therefore characterized by a small electronic polarizability ($\alpha_{Be^{2+}}$ =0.008 Å^3), which is even lower than that of characteristic network-forming cations, such as Si^{4+} ($\alpha_{Si^{4+}}$ =0.033 Å^3) [9]. Unlike other alkaline earths ions, Be^{2+} is always found to be fourfold coordinated to oxygen in crystalline oxides and to form regular BeO_4 tetrahedra [6]. This is less surprising when considering the old chemistry rule of “diagonal relationship”, that the first element in each main group shows many similarities to the 2nd element in the next group, making beryllium in many properties akin to aluminum rather than to magnesium [10]. Al_2O_3 is known as intermediate glass forming oxide, which can act either as modifier with Al^{3+} in six-fold coordination, or as glass former with Al^{3+} in four-fold coordination, while the latter is its most common role as a minor component in silicate glasses [11-13]. Al_2O_3 addition increases the glass-working range and improves mechanical and chemical resistance. Incorporation of AlO_4 tetrahedra improves the glass stability of borate and silicate glasses and hence the chemical durability [14]. Similar improvements of glass stability and mechanical properties may also be expected for BeO substitution. As shown for borate glasses, Be^{2+} takes mostly a fourfold coordination to oxygen regardless of the glass composition, and therefore it takes the role of a network-former [15]. Beryllium-alumino-silicate glasses have been reported to have high elastic moduli and strong chemical and thermal shock resistance [16]. This unusual coordination chemistry of the alkaline earth ion Be^{2+} and the associated physico-chemical properties of Be compounds make the structural study of beryllium-silicate glasses a fascinating topic.

The aim of the present work is to extend the characterization of beryllium-containing silicate glasses by exploiting the advances of modern-day characterization techniques. Structural and thermal properties analysis is performed for two different glass systems with a composition close to $35M_2O$-xBeO-(65-x)SiO_2 where the BeO content is increased at the expense of SiO_2. The first series contains a high content of sodium (35 mol% Na_2O) while a quarter of the sodium ions are substituted by lithium ions in the second series (27 Na_2O – 9 mol% Li_2O). The proposed compositions allow us to discuss not only the single alkali but also aspects of the mixed alkali effect, as well as the influence of beryllium addition on the silicate glass structure and thermal glass properties.

2. Experimental

2.1. *Glass preparation*

Two series of silicate glasses containing beryllium were prepared. The first system of glasses contains sodium oxide as flux and has the nominal composition $xBeO–(65-x)SiO_2–35Na_2O$ mol% (approximately $Be_xNa_{23.7}Si_{21.7-x}O_{54.2}$ at%, designated as xBN). The second series contains sodium and lithium oxides as fluxes and has the composition $xBeO–(64-x)SiO_2–27Na_2O–9Li_2O$ mol% (approximately $Be_xLi_{6.1}Na_{18.3}Si_{21.3-x}O_{53.9}$ at%, designated as xBNL). In both cases, x = 0, 5, 10 and 15 mol% (x = 0, 1.7, 3.4 and 5.3 at%). Respective amounts of reagents: BeO (99% Alfa Aesar), SiO_2 (99.99% ChemPur GmbH), Na_2CO_3 (99.9+% ChemPur GmbH) and Li_2CO_3 (99.999% ALDRICH) were thoroughly mixed in a fume hood. Melting was performed in Al_2O_3 crucibles at 1400-1450 ^oC for 60 min, under air atmosphere. As shown by ICP OES analysis the uptake of Al_2O_3 is significant and will thus be taken under consideration when discussing the experimental results. Melts were poured on a cold brass plate before annealing for five hours at a temperature of 400 ^oC under air. The cooling rate was 38 °C/h.

For comparison, Raman spectra from ref. [17] were included in this study. These glasses have the nominal composition $yAlO_{3/2}–(75-y)SiO_2–25Na_2O$ mol% (yAN).

2.2. *Glass characterization*

2.2.1. *XRD measurements*

Powder X-ray diffraction (XRD) technique was used to identify the amorphous structure and phase content of the samples. The XRD data were collected on a PANalytical PRO MPD instrument with Bragg-Brentano geometry and $CuK_{\alpha 1}$ radiation over a 2θ range of 10–70° at a step size of 0.013° and step time 52 sec. The XRD measurements were conducted at room temperature on powdered samples.

2.2.2. ICP OES

The chemical composition of the samples was investigated using an inductively coupled plasma optical emission spectrometer (ICP OES, Aviro 200 Perkin Elmer). Measurements were performed after dissolution of 0.05 g the respective glass powders in 5 ml of aqueous solution of HF acid (40%). All ICP OES values are listed in Table 1. The error margins of ICP-OES analysis were ± 3 % for all elements. The oxygen content was determined from the charge requirements of the analyzed cations. Periodic table mix for ICP measurements (SIGMA ALDRICH) was used as reference standards.

2.2.3. CSLM observations

The topography of samples was observed by using an Olympus LEXT OLS4000 Confocal Scanning Laser Microscope (CSLM). Color imaging was done in white LED light and 3D images were obtained using a 405 nm laser and Photomultiplier Detector. The maximum used objective lens and laser 3D image magnification was 100x, with optical magnification of 2160x. CSLM measurements were conducted on freshly fractured and alcohol cleaned samples.

2.2.4. Raman and IR spectroscopy

The structure of the glasses was studied by Raman and IR spectroscopy. Raman spectra were obtained in the range from 100 to 2000 cm^{-1} with a resolution of 2 cm^{-1} with a dispersive confocal Raman microscope (Renishaw inVia) using the 514.5 nm laser excitation line. The sample spot size of the Raman microscope is about 0.5 µm in diameter. Polarized Raman spectra were obtained in VV (parallel) and HV (cross) polarization under the 514.5 nm excitation line with longer acquisitions times. In the notations VV and HV the first letter indicates the polarization of the exciting laser beam and the second letter the polarization of the scattered light.

IR measurements were carried out on glass samples using a vacuum IR spectrometer (Bruker Vertex 80v). The spectra were taken in reflectance mode with an incidence angle of $\sim 11^{\circ}$, in the range of 30–7000 cm^{-1} with a resolution of 2 cm^{-1}. 100 scans were collected from the "as-is" surface of the quenched glass samples and the average of the scans was analyzed. Restrictions on sample size, prevented us from further polishing the as quenched samples, and instead IR spectra for the xBN and xBNL samples were obtained in the reflectance mode from the pristine glass surfaces. Contrary to Raman spectroscopy, sample preparation is an important factor in the quality of specular reflectance infrared spectra, which are ideally obtained from plane, polished sample surfaces, as in the case of the yAN series [17, 18].

The Raman and IR band positions were estimated as the mean value of observed maxima using the software Origin, with an estimated error in the band position of ± 2 cm^{-1}.

2.2.5. DTA analysis

The thermal properties of the glasses were investigated by differential thermal analysis (DTA). DTA measurements were performed up to 1000 °C on powdered samples placed in Al_2O_3 crucibles, under flowing nitrogen, with a NETZSCH STA 409PC instrument and a heating rate of 20 °Cmin^{-1}. The onset and midpoint of an endothermic drift found on the DTA curve were taken as representing T_g. The exothermic processes observed in all samples are correlated with crystallization processes. The thermal properties parameters were estimated with the use of dedicated software. The precision in the determination of thermal processes depends on the selected temperature range and varies up to ± 2 % from the determined value.

3. Results and discussion

3.1. XRD, ICP OES and Confocal microscopy

Melt quenching of beryllium-silicate glasses containing either sodium or sodium and lithium ions resulted in clear, colorless and transparent glass samples. An exemplary CSLM picture of glasses´ topography is presented in Fig. 1, for glass 0BN (Na_2O-SiO_2). The topography of other glasses looks similar. Some samples contained small air bubbles. Table 1 presents their target and measured compositions. No significant loss of the alkali (Na, Li) or alkaline earth (Be) components are observed, nor of silicate. The sample names are based on the xBeO content in mol% (x=0, 5, 10 or 15) and the series are designated considering the presence of only sodium (xBN) or sodium and lithium (xBNL). All glasses contain aluminum, which originates from the crucible material and is included in the analyzed compositions (see Table 1). It is worth to notice that the basic glasses without beryllium (0BN and 0BNL), contain only trace amounts of Al (~0.5 at% or <1 mol% Al_2O_3), while samples doped with BeO show significantly higher Al-levels. Moreover, xBN glasses exhibit on average significantly less Al than the xBNL series containing lithium. The highest dissolution of Al_2O_3 in the melt is found for glasses with the highest Be-content, for 15BNL the Al content being as high as ~11 at.%. These observations suggest that the melt with the higher oxide (M_2O+MO) content and with lower basicity (BeO and Li_2O compared to Na_2O) reacts more readily with the alumina crucible. We can only speculate about the causes of the higher aluminum solubility with higher Li_2O and BeO levels in the glasses; increasing melting temperatures with increasing BeO levels might be responsible, or a lower viscosity of the melt with BeO additions (see [19]). Interactions of glass melts with alumina crucibles have been studied in more systematic fashion before, see for example refs. [20-22].

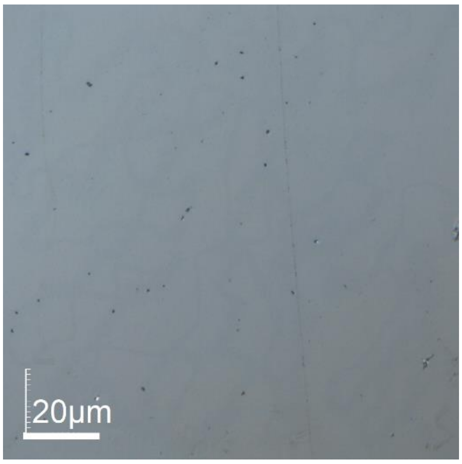

Figure 1. CSLM micrograph for fractured glass 0BN.

Table 1 Glasses ID, target and analyzed compositions. The O:Si ratio was estimated for 2 extreme cases: (i) O:Si* assumes that Al_2O_3 and BeO form $[BeO_{4/2}]^{2-}$ and $[AlO_{4/2}]^{-}$ tetrahedra first, and only the remaining O atoms modify the silicate network, and (ii) O:Si$^{\#}$ assumes that Al_2O_3 and BeO act as modifiers only, and all oxygen atoms will thus be bonded to the silicate network. For comparison, the O:Si* and O:Si$^{\#}$ values are included for glasses $yAlO_{3/2}$–(75-y)SiO_2–25Na_2O (yAN) of ref. [17].

Sample ID	Target composition (in at%)	ICP OES analyzed glass composition (in at%) $^{+}/_{-}$ 3 %	Analyzed glass composition (in mol%) error +/- 3%	O:Si* nom	O:Si* exp	*O:Si$^{\#}$ theoretical*	*O:Si$^{\#}$ estimated*
xBeO–(65-x)SiO_2–35Na_2O							
0BN	$Na_{23.3}Si_{21.7}O_{55}$	$Na_{22.4}Si_{21.1}Al_{0.5}O_{56}$	34.1Na_2O–65.1SiO_2–0.8Al_2O_3	2.53	2.60	*2.53*	*2.66*
5BN	$Be_{1.7}Na_{23.7}Si_{20.3}O_{54.2}$	$Be_{1.8}Na_{20.7}Si_{20.6}Al_{0.8}O_{56.2}$	5.4BeO-31.2Na_2O–62.1SiO_2–1.2Al_2O_3	2.50	2.48	*2.67*	*2.73*
10BN	$Be_{3.4}Na_{24.1}Si_{19}O_{53.4}$	$Be_{3.7}Na_{21.2}Si_{18.9}Al_{1.4}O_{54.8}$	10.9BeO–31.3Na_2O–55.8SiO_2–2.1Al_2O_3	2.45	2.36	*2.82*	*2.91*
15BN	$Be_{5.3}Na_{24.6}Si_{17.5}O_{52.6}$	$Be_{5.5}Na_{21.3}Si_{17.6}Al_{1.8}O_{53.9}$	15.9BeO–30.7Na_2O–50.8SiO_2–2.6Al_2O_3	2.40	2.23	*3.00*	*3.07*

xBeO–(64-x)SiO_2–27Na_2O–9Li_2O							
0BNL	$Li_6Na_{18}Si_{21.3}O_{54.7}$	$Li_{6.7}Na_{17}Si_{21.3}Al_{0.4}O_{54.6}$	10Li_2O–25.5Na_2O–63.9SiO_2–0.6Al_2O_3	2.56	2.53	*2.56*	*2.57*
5BNL	$Be_{1.7}Li_{6.1}Na_{18.3}Si_{20}O_{53.9}$	$Be_{1.7}Li_8 Na_{16.6}Si_{17}Al_{2.8}O_{53.9}$	5.2BeO–12.3Li_2O–25.6Na_2O–52.5SiO_2–4.3Al_2O_3	2.53	2.63	*2.69*	*3.16*
10BNL	$Be_{3.4}Li_{6.2}Na_{18.6}Si_{18.6}O_{53.1}$	$Be_{3.3}Li_{7.7}Na_{15.1}Si_{14.9}Al_6O_{53.1}$	10.1BeO–11.8Li_2O–23.2Na_2O–45.7SiO_2–9.2Al_2O_3	2.48	2.33	*2.85*	*3.58*
15BNL	$Be_{5.3}Li_{6.3}Na_{18.9}Si_{17.2}O_{52.3}$	$Be_{4.0}Li_{6.9}Na_{13.5}Si_{12.5}Al_{10.8}O_{52.3}$	12.5BeO–10.7Li_2O–21Na_2O–38.9SiO_2–16.8Al_2O_3	2.43	1.82	*3.04*	*4.19*
y$AlO_{3/2}$–(75-y)SiO_2–25Na_2O [17]							
0AN	$Na_{16.7}Si_{25}O_{58.3}$	Not determined	-	2.33	-	2.33	-
10AN	$Al_{3.39}Na_{16.95}Si_{22.03}O_{57.63}$		-	2.31	-	2.62	-
20AN	$Al_{6.90}Na_{17.24}Si_{18.97}O_{56.90}$		-	2.27	-	3.00	-
30AN	$Al_{10.53}Na_{17.54}Si_{15.79}O_{56.14}$		-	2.22	-	3.56	-

The XRD curves displayed in Fig. 2 for all xBN samples show a typical glass bump, which is characteristic for amorphous materials. Similar results (not presented here) were obtained for the xBNL glass series.

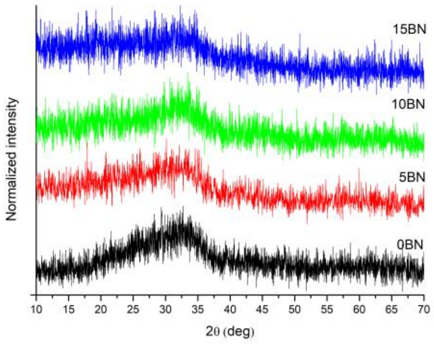

Figure 2. XRD curves for glass series xBN.

3.2. *Raman and IR spectroscopy*

The Raman and infrared spectra of all samples are shown in Fig. 3 to 5. For comparison and better understanding of the Raman and infrared results, Figures 4 and 5 include also spectra of the alumino-silicate glass series $yAlO_{3/2}$–$(75-y)SiO_2$-$25Na_2O$ (with y=0, 10, 20, 30 mol%, denoted yAN in the following discussion) from reference [17].

Before starting on the spectral interpretation, let us consider how alkaline earth modifier oxides usually modify the glass network, and what role beryllium ions take in various beryllium-bearing minerals such as Bromellite (BeO), Chrysoberyl (Al_2BeO_4) or Phenakite (Be_2SiO_4); which have been studied by Hofmeister et al. by vibrational spectroscopy [23].

(a) BeO as modifier oxide

If we assume that BeO acts as modifier oxide, all oxygen atoms from BeO modify the silicate tetrahedra and Be^{2+} ions balance the negative charge of the non-bridging oxygen atoms in silicate tetrahedra, as it is well known for Na^+ ions:

$$2[SiO_{3/2}O^-\ Na^+](Q^3) + BeO \longrightarrow SiO_{2/2}O_2^{2-}\ 2Na^+(Q^2) + SiO_{2/2}O_2^{2-}\ Be^{2+}(Q^2) \quad (1)$$

Here, the silicate network would be modified by depolymerization. The O:Si$^\#$ ratio listed in Table 1 and which correspondents to this scenario, shows an increase from 2.5 in 0BN(L) (primarily Q^3 silicate units) to 3 (primarily Q^2 silicate units) in the 15BN(L) glasses. Q^n denotes silicate tetrahedra with n bridging and $4-n$ non-bridging oxygen atoms.

(b) BeO as intermediate glass former

As mentioned earlier, the diagonal relationship predicts, in agreement with earlier studies [6], that Be^{2+} ions show a very similar behavior to Al^{3+} ions. Thus, just as aluminum forms $[AlO_{4/2}]^-$ tetrahedra in many glasses [11-13], beryllium might also contribute as intermediate oxide with $[BeO_{4/2}]^{2-}$ tetrahedra to glass formation:

$$BeO + Na_2O \quad \longrightarrow \left[BeO_{4/2}\right]^{2-} 2Na^+ \tag{2}$$

In this reaction, 2 mols of Na^+ ions are needed to charge balance one mol of $[BeO_{4/2}]^{2-}$ tetrahedral units. Therefore, less Na_2O is available to modify SiO_2 (i.e. the SiO_2:Na_2O ratio increases) and the silicate network becomes slightly more polymerized. Postulating a preferential formation of $[BeO_{4/2}]^{2-}$ units over silicate depolymerization, the O:Si* ratio (see Table 1) shows a slight decrease from 2.5 in 0BN(L) (primarily Q^3 silicate units) to 2.4 (primarily Q^3 and some Q^4 silicate units) in the 15BN(L) glasses.

(c) BeO-cluster formation in the silicate network

Finally, a third mechanism for the effect of BeO substitution for SiO_2 might be proposed. BeO can form clusters in the silicate network and Be^{2+} ions charge balance the $[BeO_{4/2}]^{2-}$ tetrahedra, as it was proposed for binary BeO-SiO_2 glasses [6]:

$$BeO + BeO \quad \longrightarrow \left[BeO_{4/2}\right]^{2-} Be^{2+} \tag{3}$$

These $[BeO_{4/2}]^{2-}$ tetrahedra, as in case (b) above, can be inserted between two neighboring Si-O-Si bridges. However, as BeO substitutes SiO_2, an excess of Na_2O would be left to modify and depolymerize the silicate network:

$$2[SiO_{3/2}O^{-}\ Na^{+}](Q^{3}) + Na_2O \quad \longrightarrow 2[SiO_{2/2}O_2^{2-}\ 2Na^{+}](Q^{2}) \qquad (4)$$

In the case of the yAN series, the same three reaction pathways (a) to (c), described above, can be discussed, although (a) should be excluded since $[AlO_{4/2}]^-$ tetrahedra formation has been verified for many of these glasses - as long as enough Na_2O or similar modifier oxides are available for $[AlO_{4/2}]^-$ tetrahedral formation [11-13, 17, 24]. However, when discussing scenario (b) it should be noted that each $[AlO_{4/2}]^-$ tetrahedral unit needs ½ Na_2O for charge balance. Since y=2x, the remaining $Na_2O:SiO_2$ ratio would decrease from 2.33 for 0AN to 2.22 for 30AN. Scenario (b) was found to explain best the spectral changes for the yAN glass series of reference [17]. The Raman spectra show a downshift and broadening as more Q^4 silicate units are converted to Q^{3Si} units and $[AlO_{4/2}]^-$ tetrahedra are inserted into the silicate network, forming Q^{3Si1Al} and Q^{2Si1Al} units. $Q^{nSin'Al}$ denotes silicate tetrahedra linked via Si-O-bridges to nSi and n'Al atoms.

3.2.1. *Polarized Raman spectra*

Polarized Raman spectra help with band assignments and can help in the identification of bands that might be otherwise hidden, for example by merging with neighboring bands or if superimposed by bands of stronger intensity. Totally symmetric modes tend to be polarized while asymmetric vibrations are depolarized, that is even in cross polarization the band intensity is higher than 75% of its intensity in parallel polarized Raman spectra. The interested reader is referred to our recent work in reference [25] for additional information on band activity in polarized Raman spectra and the respective infrared spectra. Fig. 3 shows the polarized Raman spectra of glasses xBN and xBNL for additions of x=0 and 5 mol% BeO. Let us consider first the polarized Raman spectra of the beryllium free glasses with nominal compositions $65SiO_2–35Na_2O$ (0BN) and $64SiO_2–27Na_2O-9Li_2O$ (0BNL).

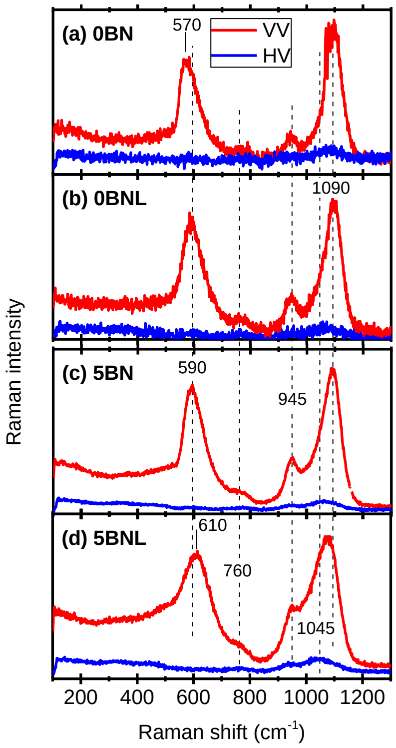

Figure 3. Polarized Raman spectra in parallel (VV, in red) and cross (HV, in blue) polarization for glasses in the BN and BNL series (for glass compositions see Table 1).

The parallel polarized (VV) spectra of the two beryllium free glasses show the strongest Raman band at 1090 cm^{-1}, which is highly polarized, and can be assigned to $Si-O^-$ stretching in Q^3 ($SiO_{3/2}O^-$) tetrahedra [17, 26-30]. All other bands are also highly polarized, and almost disappear for the spectra obtained in cross polarization (HV, Fig 3 a and b). The band at 945 cm^{-1} is due to the $Si-O^-$ stretching vibration in Q^2 tetrahedral units, $[SiO_{2/2}O_2]^{2-}$, while the least polarized bands in the Be-free glasses 0BN and 0BNL at 760 to 775 cm^{-1}, due to bending modes of Si-O-Si bridges between the silicate tetrahedra, are already of weak intensity when measured in parallel polarization [17, 26-29]. The band at ca. 570 cm^{-1}, which is due to a combination of stretching and bending vibration of Si-O-Si bridges [17, 29], shows a dependence on the degree of silicate network depolymerization and the modifier cation, and shifts to 590 cm^{-1} as 9 mol % of Na_2O is substituted by Li_2O. If we consider the band positions in the cross polarized spectra (HV), it is apparent that the position of the main band of the Si-O^- stretching mode is found at lower energies. For example the shift from 1090 cm^{-1} in the parallel polarized spectrum of 0BNL to 1064 cm^{-1} in the cross polarized spectrum, was already noted by Furukawa et al. [29] for Na_2O-SiO_2 glasses. In addition, the cross polarized spectrum shows a broadening to the lower energy side when compared to the parallel polarized spectrum.

The addition of only 5 mol% BeO results in a distinct increase in band intensities of the cross-polarized spectra, especially for the Si-O^- stretching modes at 945 and 1095 cm^{-1}. As noted for the 0BN(L) glasses, the maximum of the Si-O^- stretching band shifts in the cross polarized spectra to lower energies: from 1090 to 1063 cm^{-1} for 5BN and from 1075 to 1045 cm^{-1} for 5BNL. This shift is consistently around 30 cm^{-1}, and can originate from the effect of different charge balancing cations, i.e. either Na^+, Li^+ or Be^{2+}, on the non-bridging oxygen atoms as observed in phosphate glasses [31]. And indeed, this shift is more pronounced in the multicomponent glasses 0BNL, 5BN and 5BNL, as compared to binary sodium silicate glasses [29]. An alternative origin of this depolarized band is the formation of Q^{32} units, that is, Q^3 silicate units that are connected to Q^2 units. This additional differentiation of Raman bands has been shown useful in band separation of ion exchanged glasses [30, 32]. Indeed, the band intensity at 945 cm^{-1} is enhanced in the beryllium-containing glasses relative to Be-free glasses, and for comparable Be-levels it is higher in the Li-containing glasses than in the Li-free samples. An increase in the relative Q^2 population with BeO addition would indicate an increased silicate network modification through the oxygen atoms introduced by BeO. However, one-to-one substitution of Na_2O by Li_2O should not create more non-bridging oxygen atoms on the silicate network (ignoring here the additional 1 mol% M_2O content in the xBNL series compared to the xBN series). The higher Q^2 population at constant M_2O content can be explained by the disproportionation of Q^3 groups into Q^4 and Q^2 units when high field strength cations, such as $Li^{+,}$ are introduced into the glass [30]:

$$2\left[SiO_{3/2}O^{-}\right](Q^3) \leftrightharpoons SiO_{4/2}(Q^4) + SiO_{2/2}O_2^{2-}(Q^2) \tag{5}$$

The increased intensity at 945 cm^{-1} with BeO addition (Fig. 3c and d) shows the formation of more Q^2 groups, and this points towards a network modifying role of BeO (Eq. 1) and/or a stronger disproportionation of Q^3 to Q^4 and Q^2 (Eq. 5) due to the high field strength of the Be^{2+} ion. For a better view into these aspects we consider next the unpolarized Raman spectra of the xBN(L) series with higher BeO additions.

3.2.2. Unpolarized Raman spectra

The Raman spectra of the beryllium-free glasses $65SiO_2$–$35Na_2O$ (0BN) and $64SiO_2$–$27Na_2O$-$9Li_2O$ (0BNL) are compared in Figure 4a with the Al-free $75SiO_2$–$25Na_2O$ (0AN) glass. While the 0BN and 0BNL glasses have a similar $O:Si^{*}_{nom}$ ratio of 2.53 and 2.56 (see Table 1), respectively, a lower $O:Si^{*}$ ratio of 2.33 is found for the 0AN glass. In Figs. 4b to d the spectra of glasses with xBeO addition are compared with the Raman spectra of yAN glasses (from reference [17]). As observed in Table 1, the $O:Si^{*}$ ratio for the yAN glasses is lower than that of their corresponding in Fig. 4 glasses xBN and xBNL, indicating a lower level of modification of the silicate network in the yAN glass series. An O:Si ratio of 2.5 corresponds to a silicate glass made up entirely of Q^3 units, $SiO_{3/2}O^{-}$. The glass 0AN with an $O:Si^{*}$ ratio of 2.33 corresponds nominally to a glass consisting of two thirds of Q^3 and one third of Q^4 units and is, therefore, more polymerized than the two glasses of the beryllium-series (0BN, 0BNL). The Raman spectra in Fig. 4a show a very strong band at 1090 cm^{-1}, which arises from stretching modes of $Si\text{-}O^-$ bonds in Q^3 units, $\nu(Si\text{-}O^-)$ Q^3, in agreement with the expected glass structure [17, 29, 30, 33]. The spectrum of the glass 0AN shows in addition a pronounced contribution on the high-energy side of the 1090 cm^{-1} band, reflecting the presence of Q^4 groups, while the analogous band from Q^2 units at 945 cm^{-1} is weaker in the 0AN glass when compared to the 0BN or 0BNL glasses. Thus, it is evident from the Raman spectra that the degree of silicate network depolymerization increases in the series 0AN<0BN<0BNL in line with the trend of the $O:Si^*$ ratio. The presence of a small amount of Q^2 units in 0AN arises from the disproportionation reaction of Q^3 units, as described earlier in equation (5). Q^4 units have a much lower Raman scattering cross section compared to Q^n entities with non-bridging oxygen atoms [17], and their presence is only evident in Fig. 4a as a contribution to the high energy side of the 1090 cm^{-1} peak [17, 30]. Stretching modes of Q^2 groups in the Raman spectra of glasses 0BNL and 0BN are expected from the slight oxygen excess ($O:Si^*=2.53$ and 2.56 for 0BN and 0BNL, respectively), compared to a disilicate composition ($O:Si^*=2.50$), as well as from Q^2 contributions according to the disproportionation reaction, eq. (5).

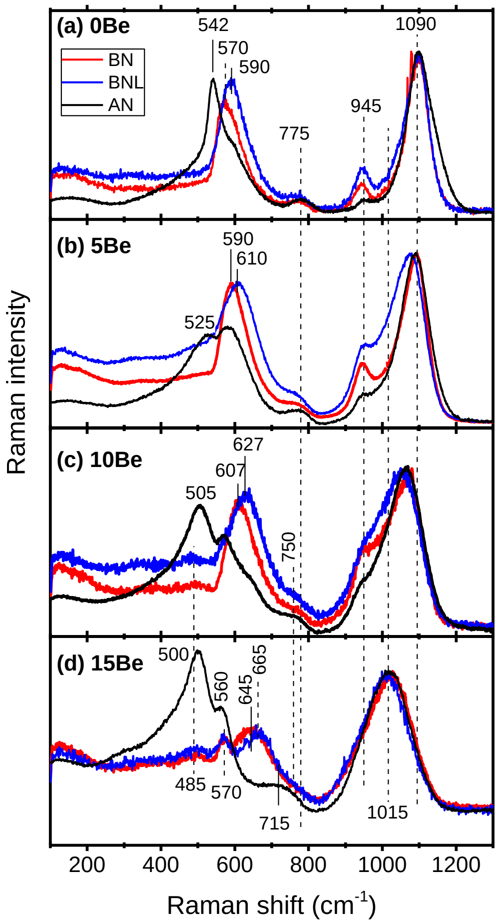

Figure 4. Raman spectra of the xBN (red), xBNL (blue) and yAN (black) glass series with increasing xBeO content: (a) 0, (b) 5, (c) 10 and (d) 15 mol% BeO; and $yAlO_{3/2}$ addition of (a) 0, (b) 10, (c) 20 and (d) 30 mol% $AlO_{3/2}$. All spectra are normalized to the intensity of the high frequency envelop at 1090 to 1015 cm^{-1}.

The weak Raman feature at 775 cm^{-1}, due to symmetric bending modes of Si-O-Si bridges, is also evident for yAN glasses [17, 29, 33]. The intense Raman envelop between 400-650 cm^{-1} in Fig. 4a reflects a combination of stretching and bending modes of the silicate network, with the position of the center of gravity close to 570 cm^{-1} which is consistent with a network that is built up predominantly by Q^3 silicate tetrahedra. The shift in position from 542 cm^{-1} (0AN) to 570 cm^{-1} (0BN) and to 590 cm^{-}

^{1} (0BNL), is consistent with increasing amounts of Q^2 units, as evident also from the intensity increase of the Si-O$^-$ stretching mode of Q^2 units at 945 cm^{-1} [29, 33].

With increasing BeO or $AlO_{3/2}$ substitution for SiO_2, similar changes are observed in the Raman spectra of the three glass series (Figs. 4b, c and d). First of all, addition of aluminum or beryllium oxides leads to a broadening of the high frequency band envelop as the main band, ν(Si-O$^-$), Q^3, downshifts from 1090 cm^{-1} to 1010 cm^{-1} and merges eventually with the 945 cm^{-1} band as the latter gains intensity. As argued in reference [17] for yAN glasses, these spectral changes can be explained by the gradual substitution of silicate Q^3 tetrahedra by $[AlO_{4/2}]^-$ tetrahedra of the same charge, and the replacement of the silicate Si-O-Si bonds by weaker Si-O-Al bonds.

The high degree of spectral overlap at the 1015 cm^{-1} envelop between the 15BN(L) glasses and the 30AN glass, reflects similarities in their glass structure; i.e., a silicate network based on Q^3 as well as Q^2 units, and for yAN glasses Q^4 units, in which charged $[BeO_{4/2}]^{2-}$ and $[AlO_{4/2}]^-$ tetrahedra are formed and are inserted in the silicate network. Thus, the composition dependence of the 800-1200 cm^{-1} envelop of the three glass series manifests the intermediate glass-forming role of both Al_2O_3 and BeO oxides. We note that coupling between stretching vibrations of Si-O and Al-O bonds, as well as between Si-O and Be-O bonds, accounts for the progressive loss of spectral details in the 850-1200 cm^{-1} envelop in Fig. 4 upon increasing the Al_2O_3 and BeO contents.

The formation of $[AlO_{4/2}]^-$ tetrahedra in yAN glasses was associated with the progressive downshift of the 775 cm^{-1} band (Si-O-Si bending) to ca. 715 cm^{-1} for the 30AN glass (Fig. 4d); the latter feature was attributed to the Al-O stretching in $[AlO_{4/2}]^-$ tetrahedra [17]. Analogous evidence for the formation of $[BeO_{4/2}]^{2-}$ tetrahedra is provided by the shoulder developing at ca. 750 cm^{-1} (seen clearly in Fig. 4c). This shoulder can be attributed to the symmetric Be-O stretching (ν_1 mode) in $[BeO_{4/2}]^{2-}$ tetrahedra reported for chrysoberyl [23], while several strong bands between 678 and 722 cm^{-1} in bromellite (BeO) have been attributed by Arguello et al. [32] and Hofmeisert et al. [23] to ν_1, ν_3, and ν_4, modes of $[BeO_{4/2}]^{2-}$ tetrahedra, bands that easily fall together even when studying a crystal. As shown by Arguello et al. [32], some of these bands are fully depolarized and will show in cross-polarized Raman spectra.

While the three glass series show similarities in their 800-1200 cm^{-1} envelop, the Raman response of yAN glasses exhibits distinct differences in the 400-700 cm^{-1} region when compared to xBN(L) glasses. Upon increasing y, the 542 cm^{-1} band of yAN glasses splits into two components and downshifts in frequency with peaks observed eventually at 500 and 560 cm^{-1} for y=30 (Fig. 4d). This trend is indicative of an increasing polymerization of the silicate network, in agreement with the decreasing value of the O:Si* ratio (Table 1). The band at 500 cm^{-1}, which is the strongest band of the 30AN glass spectrum, can be assigned to the stretching-bending vibration of Si-O-Si bridges and the one at 560 cm^{-1} to the corresponding mode of Al-O-Al bridges and/or to the breathing mode of 3-membered (Al,Si)-containing rings [34].

Contrary to the behavior of the 542 cm^{-1} band of glass AN, the 570 and 590 cm^{-1} bands of glasses BN and BNL (Fig. 4a) upshift in frequency and decrease in relative intensity upon increasing BeO content. The corresponding bands for Si-O-Si stretching-bending vibrations are measured at 590 and 610 cm^{-1} for 5Be (Fig. 4b), at 607 and 627 cm^{-1} for 10Be (Fig. 4c), and at 645 and 665 cm^{-1} for 15Be glasses in Fig. 4d, where they exhibit also strongly reduced intensity. Such a trend is fully consistent with the breaking of Si-O-Si bridges as a result of non-bridging oxygen formation adding to the Raman scattering of $[BeO_{4/2}]^{2-}$ tetrahedra between 680 and 750 cm^{-1} discussed earlier in this section. $[BeO_{4/2}]^{2-}$ insertion generates Si-O-Be bonds of unequal strength, and vibrational spectroscopy does not see $[BeO_{4/2}]^{2-}$ tetrahedral units as equal glass forming unit [23]. This leads to the apparent progressive depolymerization of the silicate network. The 570 cm^{-1} band of the 15Be spectra in Fig. 4d can be taken as analogous to the 560 cm^{-1} band of the 30AN glass, because of the presence of considerable amounts of Al_2O_3 in these BeO-containing glasses due to leaching from the alumina crucible (Table 1). The weak feature at ca. 485 cm^{-1} in Figs. 4c and 4d can be associated with the formation of 4-membered silicate rings [35]. For convenience, the assignments of Raman bands are collected in Table 2.

In concluding this section, we have shown that Al_2O_3 exhibits a clear intermediate glass-forming role while BeO appears to behave both as intermediate glass-forming and, in terms of Raman spectroscopy, as glass-modifying oxide in the silicate glasses considered here.

As discussed by Hofmeister et al. [23] for mixed Si-O-Be, only Si-O modes are visible in the high-energy region. The lighter, lower charged antagonist of the bond turns invisible. Here, a fundamental question on the definition of heteronuclear bonds arises: are oxygen atoms in asymmetric Si-O-Be bridges bridging or non-bridging in nature? We encountered a similar problem in regard to Nb-O-Si bonds, between the light, small cation Si^{4+} and the large, highly polarizable antagonist Nb^{5+} [36]).

For mixed Be/Si crystals, the high energy features of Be-O modes disappear and only Si-O stretching modes are observed [23]. Bending modes of $[BeO_{4/2}]^{2-}$ tetrahedra would also be expected at lower energies, around 338 cm^{-1} in BeO, [37], or around 450, 420, 380 and 230 cm^{-1} in chrysoberyl ($Al_2Be_2O_4$) [23]. Thus, the low energy features in the Raman spectra will be a mix of Be-, Al-, and Si-related vibrations. The 570 cm^{-1} band in Be-glasses still shows mixed stretching-bending modes of Si-O-Si bridges, though the number of these bridges decreases as $[BeO_{4/2}]^{2-}$ tetrahedra are inserted into the silicate network.

3.2.3. IR spectra

Figure 5 shows the infrared spectra of the xBN, xBNL and yAN glass series. The high frequency band envelop between 850 and 1200 cm^{-1} has the strongest intensity and shows pronounced variations with composition, as observed above for the corresponding band envelop in the Raman spectra (Fig. 4). This is in line with the origin of the infrared activity in the 850-1200 cm^{-1} range, i.e. the asymmetric stretching modes of Q^2, Q^3 and Q^4 silicate units [17]. For x=0 and x=5, surface effects, such as small ripples, lowered the glass surface quality and led to increasing background above 1200 cm^{-1} (Fig. 5). This effect may have introduced some error in the exact band positions and relative intensities of the high frequency envelop.

Glasses 0BN and 0BNL show the silicon-oxygen stretching activity of Q^3 units at 1104 and 1080 cm^{-1}, respectively, and the corresponding Q^2 activity at 960 cm^{-1} (Fig. 5a). Upon increasing BeO content, the Q^3 band shifts initially to 1070 cm^{-1} and, eventually, to 1047 cm^{-1} (Fig. 5d) and shows strong overlap with the Q^2 band (Fig. 5b). The similar trend observed for the corresponding Raman spectra was discussed in terms of the intermediate glass-forming role of BeO, with strong coupling between Be-O and Si-O vibrations. As observed in Fig. 3, the 850-1200 cm^{-1} envelop of the yAN glasses shows, in general, more pronounced shifts to lower frequencies in comparison to the xBN(L) glasses and this effect may be due stronger coupling between the Al-O and Si-O vibrations.

The presence of $[AlO_{4/2}]^{-}$ tetrahedra in yAN glasses is supported by the infrared band developing at about 700 cm^{-1}, as observed clearly in Fig. 5d for the 30AN glass

[17]. Corresponding evidence for the formation of $[BeO_{4/2}]^{2-}$ tetrahedra is given by the broad band developing at ca. 735 cm^{-1} (Fig. 5d), as this is the region where stretching modes of $[BeO_{4/2}]^{2-}$ tetrahedra are expected [23, 37].

The infrared band at about 500 cm^{-1} is due to the rocking motion of Si-O-Si bridges [17], and its composition dependence manifests the polymerization or depolymerization process undergone by the silicate network. For yAN glasses the band shifts from 475 to 460 cm^{-1} as the $AlO_{3/2}$ content increases from y=0 to y=30 mol%. This trend indicates a progressive polymerization of the silicate network as Al substitutes for Si, i.e. as a result of the glass-forming role of Al_2O_3, in agreement with the trend found in the Raman spectra for the Si-O-Si stretching-bending mode at 542-500 cm^{-1} (Fig. 5). We note that the rocking motion of Si-O-Si bridges for glasses zNa_2O-(1-z)SiO_2 was found to shift from 470 cm^{-1} (z=0) to 502 cm^{-1} (z=0.45), due to depolymerization of the silicate network induced by non-bridging oxygen formation [38]. On these grounds, the shift of the ca. 495 cm^{-1} band for 0BN(L) (Fig. 5a) to about 510 cm^{-1} for 15BN(L) (Fig. 5d) indicates a depolymerization process of the silicate network, and manifests again the glass-modifying action of BeO.

The weak features measured below 400 cm^{-1} in the far-infrared region are the cation-motion bands of Li^+ and Na^+ ions and will be considered in more detail in the following section.

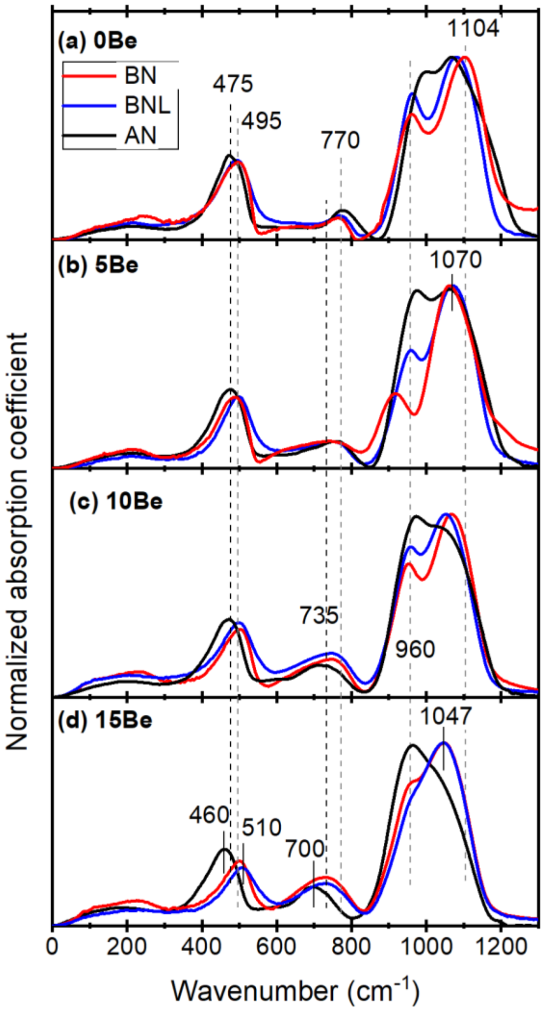

Figure 5. Infrared spectra of glasses xBN (red), xBNL (blue) and yAN (black) with increasing xBeO content: (a) 0, (b) 5, (c) 10 and (d) 15 mol% BeO, and yAlO$_{3/2}$ content: (a) 0, (b) 10, (c) 20 and (d) 30 mol% AlO$_{3/2}$. To facilitate comparison, all spectra are normalized to the intensity of the high frequency envelop 850-1200 cm^{-1}.

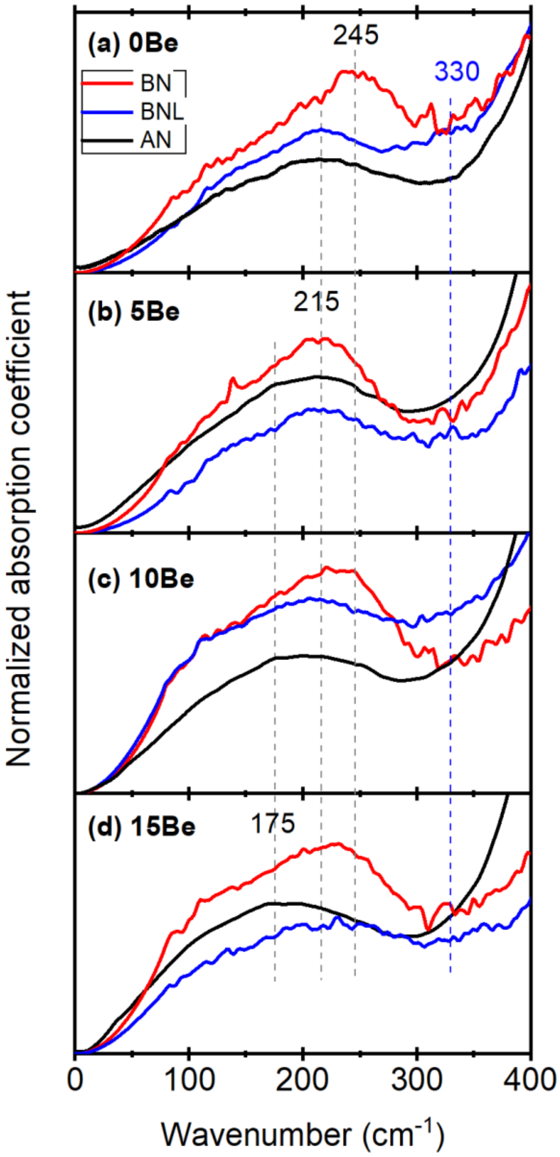

Figure 6. Far infrared spectra of glasses xBN (red), xBNL (blue) and yAN (black) showing the cation motion bands of Na^+ and Li^+ ions.

3.2.4. *Far Infrared spectra*

The far-infrared spectra are shown in Figure 6 in expanded intensity and frequency scales. For binary glasses, the vibration of Na^+ ions against their oxygen sites, ν(Na-O), is found to peak near 245 cm^{-1} for 0BN and 215 cm^{-1} for 0AN glass (Fig. 6a), in agreement with previous studies on sodium-silicate glasses [17, 38, 39]. The cation motion band of the lighter and high field strength Li^+ ion, ν(Li-O), overlaps with the Si-O-Si rocking motion band which starts around 350 cm^{-1}, though a weak distinct feature at about 330 cm^{-1} for 0BNL glass might be assigned to the vibration of Li^+ ions in their sites, ν(Li-O). In high ionic phosphate sulphate glasses, a Li^+ motion band was found at 365 cm^{-1} [40], and in borate glasses in the range 300–540 cm^{-1} depending on the Li_2O content [41]. Despite the relative noise of the spectra taken from unpolished samples, a general trend shows that the far-IR intensity reflects the changing sodium content as it decreases from 35 in xBN to 27 in xBNL and 25 mol% Na_2O in yAN. In the presence of Li^+ ions in 0BNL glass, the Na^+ ion motion band appears shifted to 215 cm^{-1} in comparison to 245 cm^{-1} in 0BN. This is another manifestation of the mixed cation effect on the dynamics of the dissimilar cations, according to which the higher-field strength cation (here Li^+) forces the low-field strength cation (here Na^+) into energetically less favored sites [42, 43].

Table 2. Raman and IR band positions and assignments for xBN(L) and yAN glasses.

Raman (± 2 cm^{-1})	**IR** (± 2 cm^{-1})	**assignment**	**references**
1150	~1170	ν(Si-O), Q^4	[17, 30]
1090	1080-1104	ν($Si-O^-$), Q^3 connected to Q^3	[17, 29, 33]
1010	~1045	ν($Si-O^-$), Q^3 connected to $[AlO_{4/2}]^-$ or $[BeO_{4/2}]^-$	[17, 44], this work
945	960	ν($Si-O^-$), Q^2	[17, 29, 33]
775	780	δ(Si-O-Si)	[17, 29, 33]
~700	700	ν(Al-O), $[AlO_{4/2}]^-$	[17, 44]

$\sim$680-750	735	ν(Be-O), $[BeO_{4/2}]^-$	[23]
500-665		Si-O-Si stretching-bending	[17, 29]
	460-510	Si-O-Si rocking motion	[17, 36]
$\sim$560, 570		Al-O-Al stretching-bending or breathing of 3-membered (Al,Si)-containing rings	[17, 34, 44]
$\sim$485		breathing of 4-membered silicate rings	[35]
	$\sim$330	ν(Li-O)	[40, 41]
	$\sim$175-245	ν(Na-O)	[17, 38, 39, 41]

As BeO or Al_2O_3 is added to the Na-silicate glass, the Na^+ motion band becomes broader and the v(Na-O) frequency shifts to lower values, at about 215 cm^{-1} for 15BNL and 175 cm^{-1} for 30AN in comparison to 245 cm^{-1} and 215 cm^{-1} for 0BN and 0AN glasses, respectively. The measured asymmetric far-IR profiles suggest the existence of a distribution of Na^+-hosting sites, which should differ mainly in their negative charge density [17]. In Be- and Al-free glasses, the Na^+ ions interact primarily with non-bridging oxygen (NBO) atoms of the silicate Q^3 and Q^2 units, and the strength of these interactions determine the value of the v(Na-O) frequency. In Be- and Al-containing glasses, the formation of $[BeO_{4/2}]^{2-}$ and $[AlO_{4/2}]^-$ tetrahedral units leads to a redistribution of part of the negative charge on these units. Thus, with respect to negative charge localization on the NBOs of Q^3 and Q^2 units, the charge becomes now delocalized on such glass-forming $[BeO_{4/2}]^{2-}$ and $[AlO_{4/2}]^-$ units. As a result, the interactions of Na^+ ions with the latter units are weaker compared to those with NBOs, and this is manifested by the broadening and downshift of the corresponding Na^+-site vibration bands (Fig. 6).

3.3. *Thermal properties*

Table 3 presents the values of thermal properties as experimentally determined: the glass transition temperature $T_{g\,onset}$, and $T_{g\,mid}$, the exothermic process onset $T_{exo,\,onset}$ and peak position $T_{exo,\,peak}$ temperatures, as well as glass stabilities S_1, S_2 for all BN(L) samples. The glass stabilities, describing the resistance to crystallization during heating, are calculated according to relations: $\mathrm{S_1 = T_{exo,\,onset} – T_{g\,onset}}$ [45] and $\mathrm{S_2 = T_{exo,\,peak} – T_{g\,onset}}$ [46].

Table 3 Thermal properties of glasses xBN(L): $T_{g\,onset}$, $T_{g\,mid}$, $T_{exo,\,onset}$, $T_{exo,\,peak}$, S_1, S_2; obtained from DTA spectra.

ID	$T_{g\,onset}$ (°C) ± 2%	$T_{g\,mid}$ (°C) ± 2%	$T_{exo,\,onset}$ (°C) ± 2%	$T_{exo,\,peak}$ (°C) ± 2%	S_1 (°C) ± 4%	S_2 (°C) ± 4%
0BN	484	495	746	788	262	304
5BN	507	512	736	786	229	279
10BN	528	543	749	786	221	258
15BN	551	563	720	748	169	197
0BNL	431	443	689	712	258	281
5BNL	456	464	663	726	207	270
10BNL	475	479	614	626	139	151
15BNL	464	467	580	590	116	126

Firstly, we discuss the results for the xBN glass series. The glass transition temperature for 0BN glass is similar to the one presented in the literature for glass $30Na_2O\text{-}70SiO_2$, with T_g = 481 °C [47]. The addition of beryllium oxide increases the glass transition temperature T_g of xBN glasses in a monotonic way (Table 3). To take into account also the Al_2O_3 amount leached into the glass from the alumina crucible, we present in Figure 7a the glass transition temperature as a function of the Be+Al content for this glass system; a linear increase of T_g with Be+Al level (in at%) is clearly demonstrated. In comparison, the T_g of binary zNa_2O-(1-z)SiO_2 glasses decreases with increasing the Na_2O content, that is with depolymerization of the glass network [47]. Contrary to Na_2O, Al_2O_3 and BeO acting as intermediate glass-forming oxides can participate in the glass network with $[AlO_{4/2}]^-$ and $[BeO_{4/2}]^{2-}$ tetrahedra which are inserted in the network and crosslink the silicate units through Si-O-Al and Si-O-Be bridges, thus causing the increase in T_g.

A significant increase in T_g by 67 °C is apparent for the 15BN glass compared to 0BN glass. Other publications reported also significant increases in T_g with Al_2O_3 dissolution from the crucible material due to the cross-linking capacity of Al^{3+} ions in glasses including phosphate [21, 48] and tellurite glasses [22]. The increase of T_g with increase in BeO content was also observed for the BeO–Al_2O_3–B_2O_3 glass system, which showed significantly higher T_g values than other equivalent glasses doped with Mg, Ca, Sr and Ca instead of Be [15].

Figure 7a shows also T_g results for glasses xBNL in which a quarter of the Na^+ ions are replaced by Li^+ ions. These glasses exhibit lower glass transition temperatures than the corresponding glasses containing only sodium (xBN). The glass 0BNL has also a lower T_g than that given in the literature for the binary $34Li_2O$-$66SiO_2$ glass (456 °C, [49]), which can be explained by the mixed alkali effect [50, 51]. Generally, a lower T_g for Li-glasses compared to Na-glasses is expected for silicates [47, 49], as is a lower T_g for mixed modifier glasses compared to binary silicates [52, 53].

The observed increase in T_g with Be+Al content in the xBNL series up to x=10 reflects again the good cross-linking ability of $[BeO_{4/2}]^{2-}$ and $[AlO_{4/2}]^-$ tetrahedra, as in glasses xBN with similar Be+Al content (Fig. 7a). However, glass 15BNL shows a reduced T_g value despite its highest Be+Al content. Such a deviation of glass 15BNL from the monotonic increase of T_g may reflect the weaker network former role of $[BeO_{4/2}]^{2-}$ and $[AlO_{4/2}]^{-}$ tetrahedra compared to SiO_4-tetrahedra, which is especially apparent in the properties of a glass where the combined Al+Be levels with 14.8 at% is higher than the analyzed Si content of 12.5 at%. The lower T_g reflects on a changing role of some Be^{2+} and / or Al^{3+} ions from glass-former to glass-modifier. The network of 15BNL, as shown by Raman and IR spectroscopy, does show only minor deviations from that of 15BN, which has much less dissolved Al_2O_3, and as discussed earlier consists predominantly of Q^2 and Q^3 silicate tetrahedra.

We can only speculate how much the dissolved Al_2O_3 content contributed to the observed property changes. Comparison of the Be-silicate series with the Be-free Al-series shows a similar effect of both substitutions for SiO_2. Only additional studies in Pt-crucible melted glasses where Al_2O_3 is stoichiometrically replaced by BeO can quantify the effect that Al_2O_3 contamination has on the properties of the Be-silicate glasses. Since many industrial produced glasses are indeed melted in Al_2O_3-containing refractory materials, the Al_2O_3-dissolution is an important factor when discussing the structure and properties of silicate and other glass systems [20-22].

Figure 7b depicts the thermal glass stability dependence on the Be+Al content for all glasses xBN(L). It is clearly shown that beryllium addition decreases the glass stability in both xBN and XBNL glass systems in approximately the same monotonic way. Nevertheless, glasses doped with lithium (BNL) show in general lower values of thermal stability than glasses containing only sodium (BN) at the same Be+Al content.

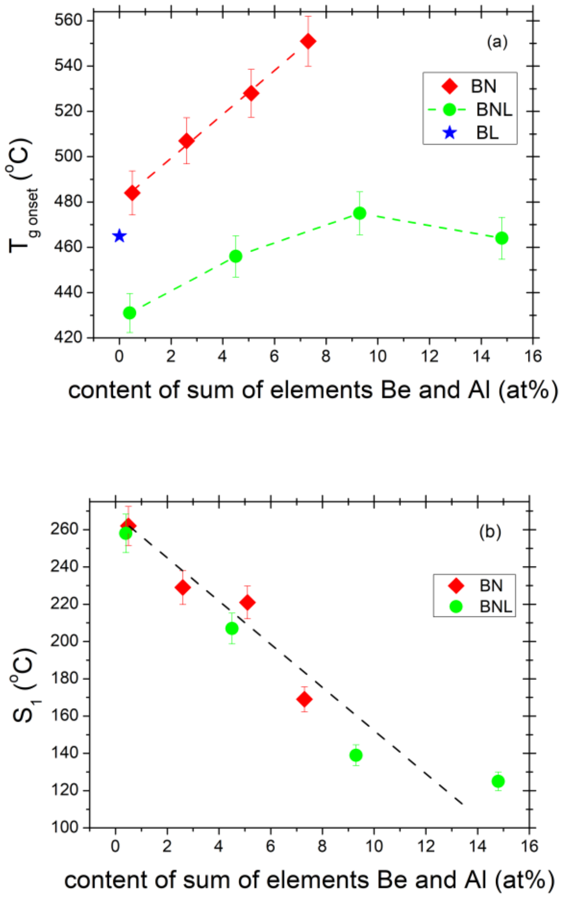

Figure 7. The dependence on the analyzed Be+Al content for (a) $T_{g\ onset}$ and (b) S_1 values for glasses xBN and xBNL studied in this work. Lines between data points show trends of thermal properties behavior and are given as guides for the eyes only. The blue star in (a) designates the T_g (465 °C) of the binary 34 Li_2O-66SiO_2 glass [49].

4. Conclusions

Two different glass series with compositions close to 35M_2O-xBeO-(65-x)SiO_2, where SiO_2 was substituted by up to 15 mol% BeO, were successfully prepared. The first glass series has a high content of Na_2O (xBN), while in the second series 9 mol% of Na_2O was replaced by Li_2O (xBNL). All glasses were found to be amorphous and contain Al, which originated from the crucible material (alumina). The Al content was found to be higher for glasses doped with Be and significantly higher for glasses containing also Li (up to 10.8 at% for glass 15BNL, though for this glass it is suspected that a fragment of the crucible broken off during melting).

The results of Raman and IR spectroscopic measurements showed many similarities between the studied xBN and xBNL glasses and a similar sodium-silicate glass series doped only with Al_2O_3 (yAN, [17]). An analogous effect on the structure of the alkali silicate network was found for BeO as shown before for $AlO_{3/2}$ substitution of SiO_2, i.e. $SiO_{4/2}$ tetrahedra are being replaced by $[BeO_{4/2}]^{2-}$ tetrahedra. This intermediate glass-forming role of BeO requires Na_2O for the formation of the $[BeO_{4/2}]^{2-}$ tetrahedra, leaving the remaining silicate network more polymerized compared to the Be-free base glass. A competing glass-modifying role of BeO takes over at increasing BeO contents and leads to the progressive destructions of Si-O-Si bridges. As $[BeO_{4/2}]^{2-}$ tetrahedra are inserted in the silicate network, Si-O-Si bridges are destroyed, and due to the asymmetric nature of the Si-O-Be bridges, IR and Raman spectra show therefore a breakup of the silicate network. Smaller, but significant changes in the glass structure are also observed when comparing glasses containing only Na^+ ions with those containing both Na^+ and Li^+ with a Na:Li ratio of 3:1.

Despite the fact that $[BeO_{4/2}]^{2-}$ tetrahedra contribute with weaker bonds to the glass network than $SiO_{4/2}$ tetrahedra, the strong cross-linking ability of $[BeO_{4/2}]^{2-}$ tetrahedra leads to a significant increase in T_g (up to 70 °C) as BeO substitutes for SiO_2 in the Na-glass series up to 15 mol% BeO. Na-Li-glasses exhibit lower T_g when compared to Na-glasses, as was expected due to the well-known mixed alkali effect. However, the increase in T_g with BeO addition was also observed for Li-containing glasses, at least for up to 10 mol% BeO substitution. The xBNL glass with the highest BeO content (x=15) and more than twice the amount of Al (in at%) showed a decreasing T_g compared to all other glasses.

Acknowledgements

SA, BJ and NAW acknowledge the financial support from the Crafoord Foundation (Grant No: 20160900). SA also acknowledges support from the ÅForsk Foundation (Grant No. 14-457) and Vinnova (Grant No. 2015-04809).

DM thanks the Knowledge Foundation (Grant No. 68110029) for financing her stay at Linnæus University.

NST and EIK acknowledge the project “Advanced Materials and Devices” (MIS 5002409) which is co-financed by Greece (General Secretariat for Research and Technology) and the European Union (European Regional Development Fund).

References

[1] C.F. Lai, A. Silverman, Beryllium glass, Journal of the American Ceramic Society, 11 (1928) 535-541.
[2] C.F. Lai, A. Silverman, Beryllium glass, II Potassium-beryllium series, Journal of the American Ceramic Society, 13 (1930) 393-398.
[3] E.F. Riebling, D.A. Duke, $BeO·Al_2O_3·SiO_2$ system: Structural relationships of crystalline, glassy, and molten beryl, Journal of Materials Science, 2 (1967) 33-39.
[4] A.G. Clare, A.C. Wright, R.N. Sinclair, A comparison of the structural role of Na^+ network modifying cations in sodium silicate and sodium fluoroberyllate glasses, Journal of Non-Crystalline Solids, 213 (1997) 321-324.
[5] T.P. Ellen, M. Costa, 14.08 - Carcinogenic Inorganic Chemicals* A2 - McQueen, Charlene A, in: Comprehensive Toxicology (Second Edition), Elsevier, Oxford, 2010, pp. 139-160.
[6] S. Sen, P. Yu, Observation of a stuffed unmodified network in beryllium silicate glasses with multinuclear NMR spectroscopy, Physical Review B, 72 (2005) 132203| 1-4.
[7] I.S. Zhidkov, A.F. Zatsepin, S.O. Cholakh, Y.A. Kuznetsova, Optical properties and structure of beryllium lead silicate glasses, in, AIP Conference Proceedings, 2014, pp. 185-191.
[8] W. Vogel, Glass Chemistry, 2 ed., Springer-Verlag, Berlin Heidelberg, 1994.
[9] V. Dimitrov, T. Komatsu, An interpretation of optical properties of oxides and oxide glasses in terms of the electronic ion polarizability and average single bond strength, Journal of the University of Chemical Technology and Metallurgy, 45 (2010) 219-250.
[10] W.B. Jensen, Holleman-Wiberg's Inorganic Chemistry (edited by Wiberg, Nils), Journal of Chemical Education, 79 (2002) 944.
[11] E. Morin, J. Wu, J. Stebbins, Modifier cation (Ba, Ca, La, Y) field strength effects on aluminum and boron coordination in aluminoborosilicate glasses: the roles of fictive temperature and boron content, Appl. Phys. A, 116 (2014) 479-490.

[12] C. Le Losq, D.R. Neuville, P. Florian, G.S. Henderson, D. Massiot, The role of Al^{3+} on rheology and structural changes in sodium silicate and aluminosilicate glasses and melts, Geochimica et Cosmochimica Acta, 126 (2014) 495-517.
[13] L.M. Thompson, J.F. Stebbins, Non-stoichiometric non-bridging oxygens and five-coordinated aluminum in alkaline earth aluminosilicate glasses: Effect of modifier cation size, Journal of Non-Crystalline Solids, 358 (2012) 1783-1789.
[14] M.I. Ojovan, W.E. Lee, An Introduction to Nuclear Waste Immobilisation, Elsevier Science, 2013.
[15] V.P. Klyuev, B.Z. Pevzner, Thermal expansion and transition temperature of glasses in the systems BeO-Al_2O_3-B_2O_3 and MgO-Al_2O_3-B_2O_3, Journal of Non-Crystalline Solids, 353 (2007) 2008-2013.
[16] W.H. Dumbaugh, Beryllium-containing high elastic modulus glasses, in, USA, 1974, Patent Version No. 224,984, US Patent Classification US. Cl. 106-52, Patent No. 3,814,611.
[17] E.I. Kamitsos, J.A. Kapoutsis, H. Jain, C.H. Hsieh, Vibrational study of the role of trivalent ions in sodium trisilicate glass, Journal of Non-Crystalline Solids, 171 (1994) 31-45.
[18] E.I. Kamitsos, Infrared Spectroscopy of Glasses, in: M. Affatigato (Ed.) Modern Glass Characterization, John Wiley & Sons, Inc., 2015, pp. 32-73.
[19] K.-U. Hess, D.B. Dingwell, S.L. Webb, The influence of alkaline-earth oxides (BeO, MgO, CaO, SrO, BaO) on the viscosity of a haplogranitic melt; systematics of non-Arrhenian behavior, European Journal of Mineralogy, 8 (1996) 371-381.
[20] I. Konidakis, C.P.E. Varsamis, E.I. Kamitsos, Effect of synthesis method on the structure and properties of AgPO3-based glasses, Journal of Non-Crystalline Solids, 357 (2011) 2684-2689.
[21] D. Palles, I. Konidakis, C.P.E. Varsamis, E.I. Kamitsos, Vibrational spectroscopic and bond valence study of structure and bonding in Al_2O_3-containing AgI-$AgPO_3$ glasses, RSC Advances, 6 (2016) 16697-16710.
[22] N.S. Tagiara, D. Palles, E.D. Simandiras, V. Psycharis, A. Kyritsis, E.I. Kamitsos, Synthesis, thermal and structural properties of pure TeO_2 glass and zinc-tellurite glasses, Journal of Non-Crystalline Solids, 457 (2017) 116-125.
[23] A.M. Hofmeister, T.C. Hoering, D. Virgo, Vibrational spectroscopy of beryllium aluminosilicates: Heat capacity calculations from band assignments, Physics and Chemistry of Minerals, 14 (1987) 205-224.
[24] C.H. Hsieh, H. Jain, A.C. Miller, E.I. Kamitsos, X-ray photoelectron-spectroscopy of Al-substituted and B-substituted sodium trisilicate glasses, Journal of Non-Crystalline Solids, 168 (1994) 247-257.
[25] I. Efthimiopoulos, D. Palles, B. Richter, U. Hoppe, D. Möncke, L. Wondraczek, S. Nolte, E.I. Kamitsos, Femtosecond laser-induced transformations in ultra-low expansion glass: Microstructure and local density variations by vibrational spectroscopy, Journal of Applied Physics, 123 (2018) 233105.
[26] P. McMillan, Structural studies of silicate-glasses and melts - applications and limitations of Raman-spectroscopy American Mineralogist, 69 (1984) 622-644.
[27] P. McMillan, B. Piriou, A. Navrotsky, A Raman-spectroscopic study of glasses along the joins silica-calcium aluminate, silica-sodium aluminate, and silica-potassium aluminate, Geochimica et Cosmochimica Acta, 46 (1982) 2021-2037.
[28] P. McMillan, A Raman-spectroscopic study of glasses in the system CaO-MgO-SiO_2, American Mineralogist, 69 (1984) 645-659.
[29] T. Furukawa, K.E. Fox, W.B. White, Raman-spectroscopic investigation of the structure of silicate-glasses. 3. Raman intensities and structural units in sodium-silicate glasses, Journal of Chemical Physics, 75 (1981) 3226-3237.
[30] E. Stavrou, D. Palles, E.I. Kamitsos, A. Lipovskii, D. Tagantsev, Y. Svirko, S. Honkanen, Vibrational study of thermally ion-exchanged sodium aluminoborosilicate glasses, Journal of Non-Crystalline Solids, 401 (2014) 232-236.
[31] L.L. Velli, C.P.E. Varsamis, E.I. Kamitsos, D. Möncke, D. Ehrt, Structural investigation of metaphosphate glasses, Physics and Chemistry of Glasses, 46 (2005) 178-181.
[32] O.N. Koroleva, V.N. Anfilogov, A. Shatskiy, K.D. Litasov, Structure of Na_2O–SiO_2 melt as a function of composition: In situ Raman spectroscopic study, Journal of Non-Crystalline Solids, 375 (2013) 62-68.

[33] P. McMillan, Structural studies of silicate glasses and melts-applications and limitations of Raman spectroscopy, American Mineralogist, 69 (1984) 622-644.

[34] I. Daniel, P. Gillet, B.T. Poe, P.F. McMillan, In-situ high-temperature Raman spectroscopic studies of aluminosilicate liquids, Physics and Chemistry of Minerals, 22 (1995) 74-86.

[35] F.L. Galeener, A.J. Leadbetter, M.W. Stringfellow, Comparison of the neutron, Raman, and infrared vibrational-spectra of vitreous SiO_2, GeO_2, and BeF_2, Physical Review B, 27 (1983) 1052-1078.

[36] D. Möncke, R. Ehrt, D. Palles, I. Efthimiopoulos, E.I. Kamitsos, M. Johannes, A multi technique study of a new lithium disilicate glass-ceramic spray-coated on ZrO_2 substrate for dental restoration, Biomedical Glasses, 3 (2017) 41-55.

[37] C.A. Arguello, D.L. Rousseau, S.P.S. Porto, First-Order Raman Effect in Wurtzite-Type Crystals, Physical Review, 181 (1969) 1351-1363.

[38] M.D. Ingram, J.E. Davidson, A.M. Coats, E.I. Kamitsos, J.A. Kapoutsis, Origins of anomalous mixed-alkali effects in ion-exchanged glasses, Glass Science and Technology-Glastechnische Berichte, 73 (2000) 89-104.

[39] E.I. Kamitsos, W.M. Risen, Vibrational-spectra of single and mixed alkali pentasilicate glasses Journal of Non-Crystalline Solids, 65 (1984) 333-354.

[40] A. Thieme, D. Möncke, R. Limbach, S. Fuhrmann, E.I. Kamitsos, L. Wondraczek, Structure and properties of alkali and silver sulfophosphate glasses, Journal of Non-Crystalline Solids, 410 (2015) 142-150.

[41] E.I. Kamitsos, M.A. Karakassides, G.D. Chryssikos, Far-infrared spectra of binary alkali borate glasses, Solid State Ionics, 28 (1988) 687-692.

[42] K. Griebenow, U. Hoppe, D. Möncke, E.I. Kamitsos, L. Wondraczek, Transition-metal incorporation and Co-Sr/Mn-Sr mixed-modifier effect in metaphosphate glasses, Journal of Non-Crystalline Solids, 460 (2017) 136-145.

[43] A. Vegiri, C.P.E. Varsamis, E.I. Kamitsos, Molecular dynamics investigation of mixed-alkali borate glasses: Short-range order structure and alkali-ion environments, Physical Review B, 80 (2009) 184202|1-12.

[44] C.I. Merzbacher, W.B. White, The structure of alkaline earth aluminosilicate glasses as determined by vibrational spectroscopy, Journal of Non-Crystalline Solids, 130 (1991) 18-34.

[45] A.R. Boccaccini, D.S. Brauer, L. Hupa, Bioactive Glasses: Fundamentals, Technology and Applications, Royal Society of Chemistry, 2016.

[46] V. Simon, D. Muresan, A. Takacs, M. Neumann, S. Simon, Local order changes induced in calcium–sodium–phosphate glasses by transition metals, Solid State Ionics, 178 (2007) 221-225.

[47] E.V. Belova, Y.A. Kolyagin, I.A. Uspenskaya, Structure and glass transition temperature of sodium-silicate glasses doped with iron, Journal of Non-Crystalline Solids, 423-424 (2015) 50-57.

[48] I. Konidakis, S. Psilodimitrakopoulos, K. Kosma, A. Lemonis, E. Stratakis, Effect of composition and temperature on the second harmonic generation in silver phosphate glasses, Optical Materials, 75 (2018) 796-801.

[49] T. Seuthe, M. Grehn, A. Mermillod-Blondin, H.J. Eichler, J. Bonse, M. Eberstein, Structural modifications of binary lithium silicate glasses upon femtosecond laser pulse irradiation probed by micro-Raman spectroscopy, Opt. Mater. Express, 3 (2013) 755-764.

[50] L. Bih, L. Abbas, S. Mohdachi, A. Nadiri, Thermal and electrical properties of mixed alkali in Li_2O–Na_2O–WO_3–P_2O_5 glasses, J Mol Struct, 891 (2008) 173-177.

[51] W. Zhifang, Z. Nai, M. Bo, S. Zhongxin, Study of the mixed alkali effect on chemical durability of alkali silicate glasses, Journal of Non-Crystalline Solids, 84 (1986) 468-476.

[52] D.E. Day, Mixed alkali glasses — Their properties and uses, Journal of Non-Crystalline Solids, 21 (1976) 343-372.

[53] S. Zhitao, L. Changjiu, T. Haizheng, Mixed alkaline-earth effect on the mechanical and rheological properties of Ca–Mg silicate glasses, Journal of the American Ceramic Society, 100 (2017) 4570-4580.